Proceedings of the ASME 2010 3rd Joint US-European Fluids Engineering Summer Meeting and
8th International Conference on Nanochannels, Microchannels, and Minichannels
FEDSM-ICNMM2010
August 1-5, 2010, Montreal, Canada

FEDSM-ICNMM2010-30477

# ANALYSIS OF INDUCED VIBRATIONS IN FULLY-DEVELOPED TURBULENT PIPE FLOW USING A COUPLED LES AND FEA APPROACH

**Thomas Shurtz**
Purdue University
West Lafayette, IN, USA

**Daniel Maynes**
Brigham Young University
Provo, Utah, USA

**Jonathan Blotter**
Brigham Young University
Provo, Utah, USA

## ABSTRACT

This paper presents an approach using numerical simulations that have been used to characterize pipe vibration resulting from fully developed turbulent flow in a straight pipe. The vibration levels as indicated by; pipe surface displacement, velocity, and acceleration are characterized in terms of the influences of geometric and material properties of the pipe, and the effects of varying flow velocity, fluid density and viscosity have considered Reynold's numbers ranging from $9.1x10^4$ – $1.14x10^6$. A large eddy simulation fluid model was coupled with a finite element structural model to simulate the fluid structure interaction using both one-way and two-way coupled techniques. The one-way technique passes the spatially and temporally varying wall pressure from a completed flow solution with fixed wall boundaries to the structural model. The structural model is then solved for wall displacements. The two-way technique involves the additional passing of wall displacement back to the fluid model which is then resolved given the new boundary location. The structural and fluid models are thus continually updated until convergence is reached at each time step. The results indicate a strong nearly quadratic dependence of pipe wall displacement on fluid average velocity. This relationship has also been verified in experimental investigations of pipe vibration. The results also indicate the pipe vibration has a power law type dependence on several variables. Dependencies on investigated variables are non-dimensionalized and assembled to develop a functional relationship that characterizes turbulence induced pipe vibration.

## 1.0 INTRODUCTION

Flow induced pipe vibration is a phenomenon that is readily observed in almost any pipe system that involves fluid motion. This paper focuses specifically on the topic of pipe vibration caused by turbulent fluid flow through a pipe. While this type of flow induced vibration is easily observed and has been the subject of some investigation, the phenomenon has not been well characterized. In industrial applications vibration can result in fatigue failure of pipe systems requiring costly maintenance and repairs [1]. With a more complete understanding of how pipe vibration is related to other variables, design tools for vibration resistant systems could be developed. Non-intrusive flow measurement techniques relying on vibration measurements could also be improved with a set of functional relationships tying vibration level and flow rate to other important variables [2].

Several of the variables that exert influence have been explored by other researchers [3-13]. Analytical, experimental, and numerical research efforts in this field have been able to identify some basic relationships describing the dependence of pipe vibration level on flow parameters and pipe geometry [6, 7, 11]. Each of the research approaches has inherent limitations and advantages, but none have resulted in a clear or complete picture or set of relations that describe pipe vibration in terms of the many influential parameters.

Analytical approaches allow precise functional relationships to be determined quickly, and do not require any expensive equipment. However, these approaches only account for average pressure and wall shear stress in the fluid and are unable to include the unsteady effects of turbulence. Experimental efforts to create and measure turbulent flow induced vibrating pipe systems provide results with direct application to industry, but can be time consuming and expensive. They are also limited by the available pipe materials and fluids, making controlled variation of parameters difficult. It is also often impossible to isolate one particular variable without affecting others. Experimental systems are susceptible to vibration from other sources, such as pump or valve noise, or entire facility vibration from traffic or machinery. Previous results from experiments such as those performed by Evans [7] are valuable for comparison, but are certainly limited in coverage. Numerical efforts at modeling a coupled system that includes time accurate turbulent fluid flow and dynamic pipe response have had some success, but have generally been limited by available computational power. Limitations on processor speed, system memory, and storage capacity have made numerical techniques useful only for simple geometries and low Reynolds numbers. While recent advances in computer technology have expanded the range of usefulness for these techniques, they have not yet been applied to developing a complete set of functional relationships that characterize pipe vibration caused by fully developed turbulent flow.

The objective of this work is to provide a more complete characterization of fully developed turbulent flow induced pipe vibration than currently exists. Although pipe vibration is usually dominated by contributions from complexities in pipe geometry such as elbows and tees, the vibration due to turbulent flow through a straight pipe segment is the focus of this research. The straight pipe case provides a baseline model that can be realistically explored using computational fluid dynamics (CFD). The functional relationships that characterize the phenomenon are determined using a numerical model coupling turbulent fluid flow with a dynamic pipe structure. The model uses a combination of large eddy simulation (LES) to solve for the time varying pressure field in the fluid domain, and finite element analysis (FEA) to solve for the transient structural response of the pipe. The effects of the most influential variables are explored by independently adjusting each. The final goal of the research is to assemble a set of functional relationships that can be used as a design tool, and with further application in improving non-intrusive flow measurement techniques. An additional objective is to develop a methodology which can be used for additional exploration of complex variable interactions so the functional relationships can continually be expanded and improved.

## 2.0 METHOD

### *2.1 LES Fluid Model*

The use of LES as a turbulence model is based on the concept that turbulent flows contain a wide range of length and time scales. The largest eddies, having dynamic and geometric properties related to the mean fluid flow, contain more energy than the smallest eddies. The LES approach makes use of this fact by applying spatial filters to the governing equations to remove, and therefore model, the smallest eddies while the large eddies are numerically simulated. This model requires less computation than direct numerical simulation (DNS) which does not filter the equations and resolves all scales of turbulence. The LES model provides the ability to resolve pressure fluctuations while allowing solutions on modest computer hardware. The Smagorinsky[14] model was used as the sub-grid-scale model in this work. All modeling of the fluid domain was done using the ANSYS CFX program because it not only allows the required LES turbulence model, but it allows direct two-way coupling with the ANSYS® Multiphysics™ structural FEA model [15].

For the model used in this research the domain was a cylinder 0.3 m long and .1015 m in diameter representing a section of the interior of a pipe. Other researchers have found that pipe lengths of 4/3D [11], 5D [16], and 2πD [17], where D is the diameter, produce adequate results. The length of pipe chosen for these simulations is approximately 3D, or slightly shorter than that suggested by Eggels [16] but significantly longer than that used by Pittard [11]. Although Pittard justified the use of a shorter pipe, the longer pipe was used here to increase the accuracy of the results.

An O-grid type mesh was used which surrounds an H-grid uniform square central region. This allows the grid to be uniformly spaced and perpendicular at the cylindrical walls. The wall region used a slight inflation layer in the radial direction to allow better resolution of the high velocity gradients there. The square central region was 60 by 60 nodes. The O-grid ring that transitions from the square central region to the cylindrical wall contains 30 radial nodes and 236 circumferential nodes. There are 180 nodes in the axial direction. A view of the mesh as seen from the axial direction is shown in Fig. 1. This mesh contains a total of 1,879,920 nodes and 1,848,175 hexahedral elements. The mesh contains 42,480 nodes on the wall where pressure information can be extracted or passed to the FEA solver in the coupling procedure.

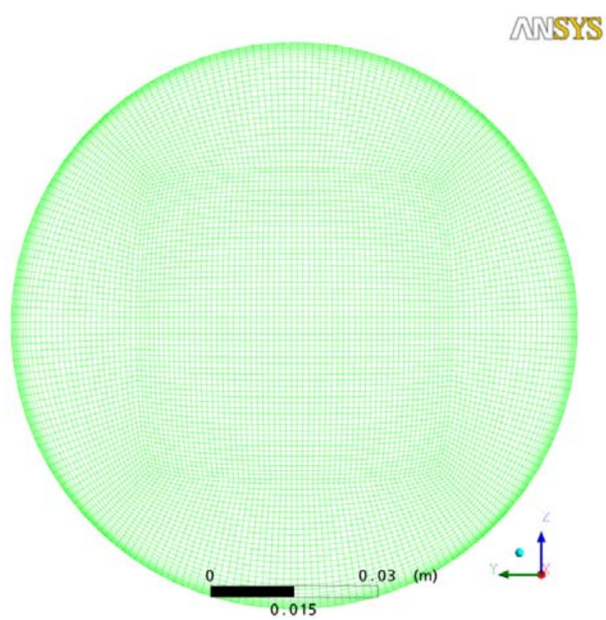


**Figure 1, Mesh used for LES Simulations**

 

Recommendations for the minimum grid spacing at the wall for LES models to be able to resolve a boundary layer are given by Piomelli [18]. Wall grid spacing suggestions are given in dimensionless form using the friction velocity, $u_\tau$, defined as $u_\tau = U\sqrt{(f/8)}$, where $U$ is the average velocity and $f$ is the Darcy friction factor. The dimensionless wall grid spacing in three directions is given by: $r^+ = r\ (u_\tau/\nu)$, $z^+ = \Delta z\ (u_\tau/\nu)$, and $R\theta^+ = R\Delta\theta(u_\tau/\nu)$, where $r$ is the perpendicular distance to the wall, $\Delta z$ is the axial grid spacing, $R\Delta\theta$ is the azimuthal grid spacing, and $\nu$ is the kinematic viscosity. Piomelli suggests using minimum values of $r^+ \leq 1$, $z^+ \approx$ 50-100, and $R\theta^+ \approx$ 15-40. Rudman used slightly higher values but was still able to get results that compared well with experimental data [17]. The wall grid spacing of this mesh is insufficient to fully resolve the near wall region. The model therefore requires the use of significant wall modeling which assumes a turbulent boundary layer type velocity profile in the near wall region. The wall spacing of the grid is shown in Table 1 in terms of wall units and compared to the dimensionless wall spacing used in studies by Pittard[11].

**Table 1, Dimensionless Grid Spacing at Wall**

| | $r^+$ | $z^+$ | $R\theta^+$ |
|---|---|---|---|
| Present Simulations $Re_D = 1.14\text{x}10^6$ | 80 | 690 | 550 |
| Present Simulations $Re_D = 9.1\text{x}10^4$ | 8.5 | 70 | 57 |
| Pittard $Re_D = 4.15\text{x}10^5$ | 279 | 284 | 284 |
| Pittard $Re_D = 8.3\text{x}10^4$ | 64 | 65 | 65 |

The LES model used a no-slip boundary condition on the pipe wall, and a periodic condition with specified mass flux at the inlet and outlet. The flow field was initialized to a uniform average velocity in the axial direction with 10% random fluctuations added in all 3 directions. The solver was then run until a pseudo-steady turbulent velocity profile developed, and the random fluctuations had developed into turbulent fluctuations. This fully developed flow field was then used as the initial condition for the simulations. Statistically steady conditions for wall shear stress and velocity profile were reached after approximately 5000 timesteps. The LES simulation used for this research was repeated for eight different Reynolds numbers, each using the same mesh, boundary conditions, and solver conditions shown in Table 2. All of the simulations assumed an incompressible fluid, and do not account for acoustic effects. The Reynold's number was varied by using velocities ranging from 1-10 m/s and holding the fluid density constant at 997 kg/m$^3$, and viscosity constant at 8.9x10$^{-4}$ Pa·s.

**Table 2, Solver Settings Used for All Simulations**

| Setting | Value |
|---|---|
| Smagorinsky Constant | 0.1 |
| Advection Scheme | 2$^{nd}$ Order Central Difference |
| Transient Scheme | 2$^{nd}$ Order Backward Euler |
| Average Courant Number | 0.6 |

### *2.2 LES Model Verification*

The LES model was verified by performing a grid refinement study. The previously described mesh that was used for all of the simulations contains approximately 1.9x10$^6$ nodes. Two additional meshes were produced with the same general O-grid structure, but containing fewer nodes, and therefore larger mesh spacing in all dimensions. The other meshes contain approximately 6x10$^4$ and 4x10$^5$ nodes respectively. The solutions on each of the three meshes were compared using the time averaged velocity profile, wall shear stress, and wall pressure fluctuations. The velocity profiles are shown in Fig. 2. The maximum velocity difference between the coarse mesh and fine mesh is about 4%, and the maximum difference between the medium mesh and fine mesh is 2%.

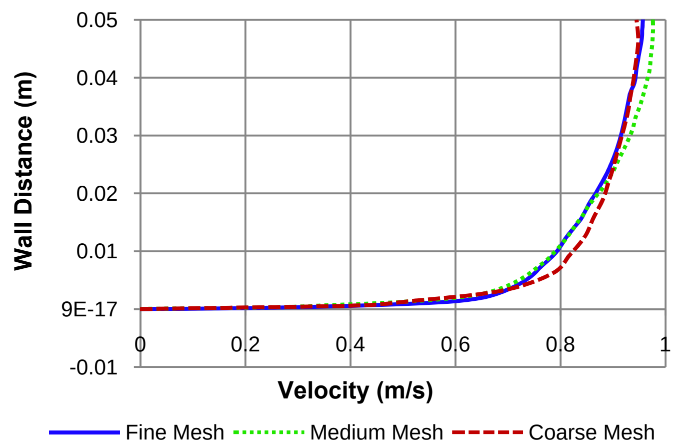


**Figure 2, Velocity profile comparison at Re = 91,000**

Table 3 shows the difference in average wall shear stress for the different grids. The wall shear stress difference between the medium mesh and fine mesh are nearly negligible due to the operation of the wall function. Although it may appear the coarse grid is sufficient, the fine grid is used to keep the near wall $r^+$value low for higher Reynolds number simulations.

**Table 3, Wall shear stress for different meshes.**
***Re* = 91,000**

| Number of Nodes | Wall Shear Stress | % Difference from Fine Mesh Solution |
|---|---|---|
| 60,000 | 1.66 Pa | +3.75% |
| 400,000 | 1.59 Pa | -0.63% |
| 1,900,000 | 1.60 Pa | - |

Because the pressure fluctuations at the wall are the driving force for pipe vibration, it is useful to consider how sensitive the amplitude of the pressure fluctuations is to the grid size. The averaged standard deviation of the wall pressure fluctuations, $P'$, is shown in Table 4 for the three meshes.

**Table 4, RMS Pressure fluctuation for different meshes**

| Number of Nodes | $P'$ | % Difference from Fine Mesh Solution |
|---|---|---|
| 60,000 | 4.49 Pa | -0.44% |
| 400,000 | 4.54 Pa | +0.67% |
| 1,900,000 | 4.51 Pa | - |

The mesh refinement study concludes that the mesh used for the simulations is adequate for calculating the pressure fluctuations needed for driving the structural pipe model. In addition to mesh refinement, the effects of timestep size were also analyzed. The use of a larger timestep than that required for a CFL number of 0.6 results in instabilities. A smaller timestep was found to cause no detectible change in the solution, so the timestep size used for the simulations is sufficient.

### *2.3 LES Model Validation*

The LES model used here has been validated using two comparisons to empirical data. Guo and Julien [19] proposed a velocity profile relation that has been shown to fit experimental pipe data very well everywhere except very near the wall. This modified log-wake law is:

$$u^+ = \frac{1}{0.41}\ln r^+ + 5.0 + 2\sin^2\frac{\pi\xi}{2} - \frac{1}{0.41}\frac{\xi^3}{3} \qquad (1)$$

where $\xi$ is the wall distance divided by the pipe radius. The velocity profile for the case with $Re_D$= 1.14x10$^6$ is compared with the log-wake law in Fig. 3. The LES model relies on the solver wall function which influences the velocity profile nearest the wall. The rest of the velocity profile fits the log-wake law very well, indicating that the LES model is representing physical pipe flow appropriately.

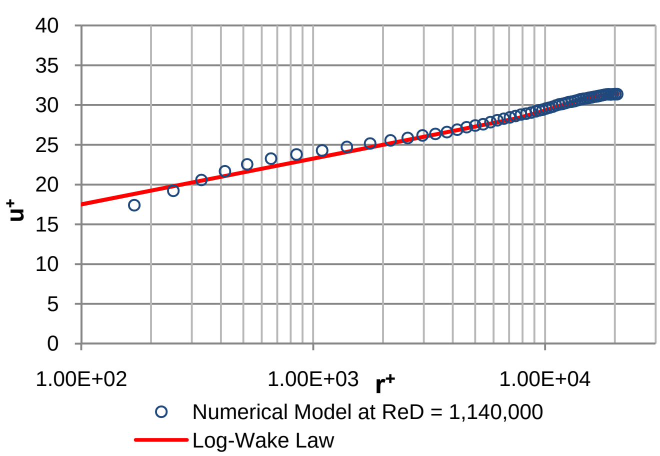


**Figure 3, $u^+$ vs. $r^+$ at $Re$ = 1.14x10$^6$**

The LES model was also validated by comparing the Darcy friction factor of the model with the measured friction factor for a smooth pipe. Experimental data has been obtained for a wide range of Reynolds numbers and can be found using the classical Colebrook equation [20], which for a smooth pipe is $\sqrt{(4/f)} = 1.5635 \ln{(Re/7)}$. The friction factor in the LES simulations was determined from the wall shear stress and is compared to those from the Colebrook equation for several Reynolds numbers in Table 5. With a maximum relative error of less than 10% the numerical results are within the uncertainty range of the experimental data, again indicating an appropriate model of the physical system.

**Table 5, Friction factor comparison with experimental data**

| Reynolds Number | LES model | Colebrook Equation | Relative Error |
|---|---|---|---|
| 91,000 | 0.0201 | 0.0182 | 8.4% |
| 227,000 | 0.0163 | 0.0152 | 5.0% |
| 455,000 | 0.0138 | 0.0133 | 2.2% |
| 1,140,000 | 0.0115 | 0.0114 | 1.2% |

### *2.4 Coupling with FEA model*

The LES solution for the fluid domain can be coupled to an FEA structural model of a pipe. Two FEA pipe models were used in this research. A short pipe model with the same dimensions as the fluid domain (L/D = 3) was constructed with fixed conditions on both ends to model a very stiff pipe segment. A long pipe model (L/D = 24) with simply supported ends was constructed to explore the effect of support spacing and pipe inertia. Both FEA models use ANSYS shell63 elements which work well for thin structures. The short model has 59 elements in the circumferential direction and 45 elements in the axial direction. The long pipe model has 59 circumferential elements and 359 axial elements. The models both allow variation of material density ($\rho_{eq}$), elastic modulus ($E$), thickness ($t$), and material damping coefficient ($\beta$). A range of values for each of these parameters was explored using the long pipe model. The short pipe model was found to be stiff enough to respond instantaneously to temporal changes in the pressure field, making its response independent of material density and damping. The thickness and elastic modulus were therefore the only parameters explored using the short model.

One goal of this research was to determine the validity of a one-way coupling approach for this type of modeling. A one-way approach assumes that although pressure fluctuations in the fluid cause the structure to deform, this deformation does not influence the flow field. This approach is advantageous because it allows a single, computationally expensive LES solution to be used for a wide range of FEA simulations. The one-way solution procedure used for this research consists of applying the pressure fluctuations from a completed LES solution as a force distribution on the FEA model. For the long pipe model, at each time step the instantaneous pressure field was applied periodically in the axial direction to cover the entire length of pipe.

A two-way procedure is necessary when the structural deformation will affect the flow field. The two-way procedure was used as a way to validate the one-way FSI (fluid structure interaction) model by determining the magnitude of the difference in results. ANSYS has built in capability for two-way coupling, which makes the process easy to implement, but very time consuming to compute. The pressure field from the fluid simulation is first calculated and interpolated so it can be applied to the structural model. The structural model then responds to the change in applied loads. The structural deformation is then interpolated and applied as a mesh deformation to the fluid domain. The fluid domain is the re-solved to determine the pressure field. This process is repeated at each timestep until no additional change is produced in the pressure field.

The two-way approach was used for a single case with a Reynolds number of 227,000. The elastic modulus of the 0.1015 m diameter pipe was set to 3.7 GPa and the wall thickness was set to 6 mm. The pipe material density for the two-way model was set to 1300 kg/m$^3$. The short pipe model was used with no damping coefficient specified. The results of the two-way simulation were then compared to a one-way simulation using the same parameters. The pipe wall motion was first compared by plotting the time series displacement calculated by both solutions. Figure 4 shows this comparison.

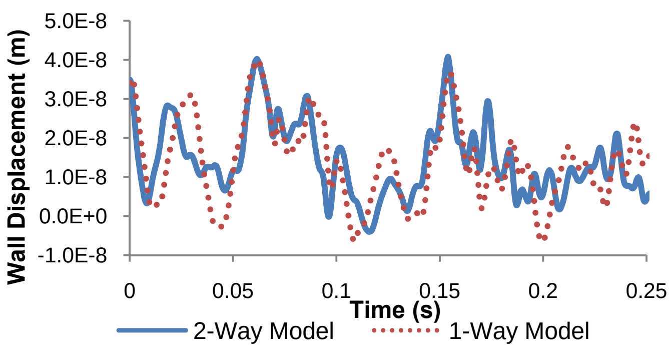


**Figure 4, Comparison of One-Way and Two-Way Simulation Wall Displacement as a Function of Time. *Re* = 2.27x10$^4$, *D* = 0.015 m, *t* = 6 mm, *E* = 3.7 GPa, *ρ* = 1300 kg/m$^3$**

The solutions appear similar, although the instantaneous wall displacement is not expected to match. Because of the chaotic nature of turbulence, even very small changes in the boundary conditions or locations can lead to large changes in instantaneous values in the flow field, especially after a long time. This would be expected to in turn cause changes in the instantaneous values of the structural solution which are illustrated in Fig. 4. A more important measure of the difference between the two methods is to compare statistical values by looking at the standard deviation of the displacement ($\delta'$), velocity ($V'$), and acceleration ($A'$). The values for these dependant variables were determined by averaging over four locations on the center of the pipe wall (top, bottom, left, and right). The values are shown in Table 6.

**Table 6, Coupling Technique Comparison Summary**

| Coupling Technique | $\delta'$(nm) | $V'$(μm/s) | $A'$(m/s$^2$) |
|---|---|---|---|
| One-Way | 9.77 | 2.89 | 0.00349 |
| Two-Way | 10.3 | 2.9 | 0.00340 |
| % Difference | 5.1% | 0.3% | 2.6% |

The maximum relative difference between the two techniques occurs for the standard deviation of wall displacement at just over 5%. Because the difference here between the two techniques is negligible relative to the expected differences from investigated parameter variation, the much faster one-way model was subsequently used.

## 3.0 RESULTS

Figure 5 displays the relationship between the Reynold's number, which was changed to produce the various flow solutions, and the standard deviation of the dimensionless wall pressure fluctuations, $C_p'$, averaged over the entire pipe wall. Also shown on this plot is the average wall friction coefficient, $C_f$. The pressure fluctuations can be fit with a power law curve with $R^2 = 0.9997$ indicating that they vary with ${Re_D}^{-0.27}$. This scales very similarly with the average wall friction coefficient which varies with ${Re_D}^{-0.23}$, indicating that the wall shear stress is likely the driving factor in determining the level of the pressure fluctuations. The values of wall shear stress determined in these simulations are those caused by a smooth wall. A rough walled pipe would be expected to yield behavior with less dependence on Reynold's number.

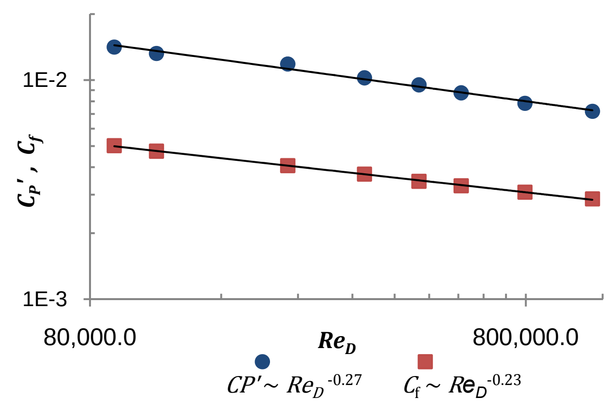


**Figure 5, $C_p'$ and $C_f$ as functions of Reynold's number in a pipe having *D* = 0.1015 m with water as the working fluid.**

The spatial correlation of the pressure fluctuations on the wall indicates that the pressure is only correlated for the relatively short scales typical of turbulence. The correlation coefficient, $C_u$ is shown as a function of separation length, Δ in both the axial (streamwise) and circumferential directions in Fig. 6. The pressure signals only show correlation for separation distances less than 6% of a diameter in the axial direction, and less than about 30% of a diameter around the circumferential direction.

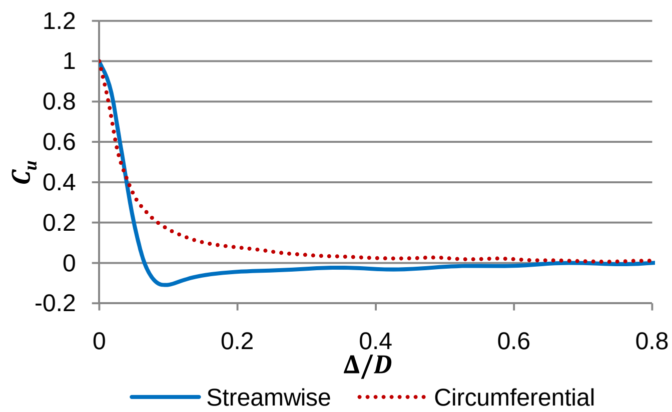


**Figure 6, Correlation as a function of separation length for the wall pressure fluctuations**

### *3.1 Short Pipe*

The short pipe has very high natural frequencies and is stiff enough to respond immediately to the changes in pressure from the fluid solution. Because the pipe wall responds so quickly, a full transient analysis of the short pipe was found to yield the same results as a static analysis. The time series wall displacement is taken from four nodes (top, bottom, front and back) situated around the domain, halfway between the inlet and outlet. The frequency content of the displacement at these four locations is averaged and presented in Fig. 7. There is some noise because of the relatively short (1/10 s) sample and averaging over only four nodes, but the trend is clear. The pipe wall displacement exhibits nominally the same characteristic frequency content as the wall pressure, but with reduced response to high frequencies. This may be due to the fact that the pipe wall averages out the smallest spatial pressure variations that correspond to the highest frequency fluctuations.

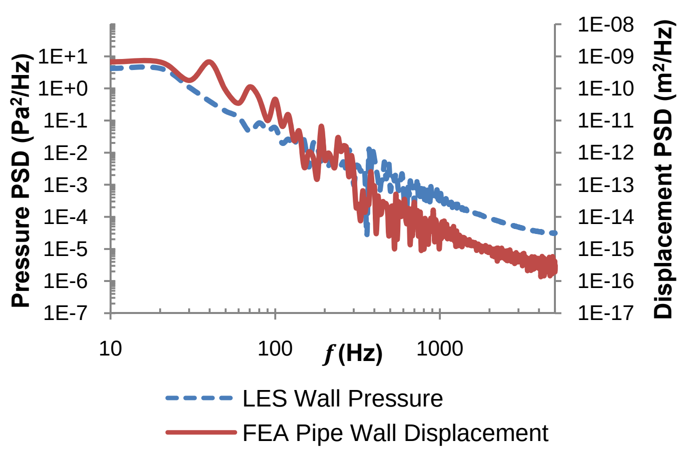


**Figure 7, Short pipe pressure and wall displacement PSD for *Re* = *1.14x10*$^6$, *D* = 0.1015 m, *t* = 3 mm, *E* = 3.7 GPa**

Another behavior of the short pipe is its tendency to respond to local pressure variations, undergoing shell-type deformations. Rather than large portions of the pipe moving together as in bending, small areas of the surface deflect relative to adjacent areas producing an unordered pattern of valleys and peaks. Figure 8 shows an image of the short pipe with exaggerated deflection and color contours of the instantaneous displacement magnitude. This localized deflection was observed to dominate the short pipe motion in all of the simulations performed with this model.

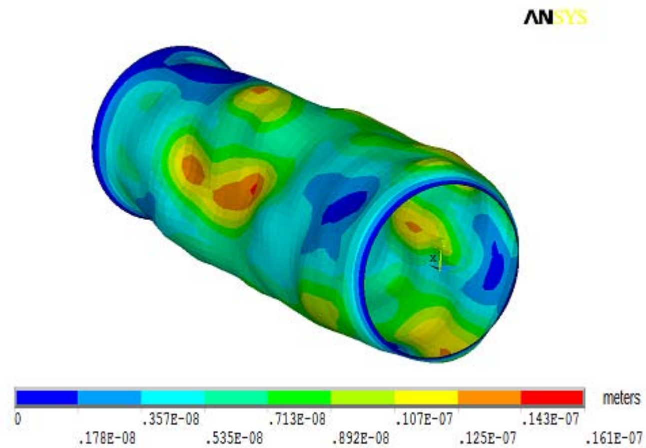


**Figure 8, Short pipe surface deflection pattern for *Re* = *1.14x10*$^6$, *D* = 0.1015 m, *t* = 3mm, *E* = 3.7 GPa**

### *3.2 Long Pipe*

The long pipe model has lower natural frequencies and is not stiff enough to respond instantaneously to the changing pressure load. This inertial effect required the use of a full transient analysis. Due to the inclusion of inertial effects in the long pipe model, the pipe responds naturally better to certain frequencies than others. The effect is to amplify the pipe wall motion in certain bands of the broad spectrum over which it is excited by the fluctuating pressure. This effect is illustrated in Fig. 9, which shows the spectral density of the pressure fluctuations overlaid on the spectral density of the pipe wall displacement response, with vertical bands indicating natural frequencies predicted by a modal analysis. As seen with the short pipe frequency response, the long pipe displacement spectrum has the same characteristic roll-off with increasing frequency, including reduced response at the highest frequencies. However, the long pipe also has a clear region of enhanced response which appears to coincide with the natural frequencies determined through a modal analysis, although significant noise prevents observation of any clearly defined peaks.

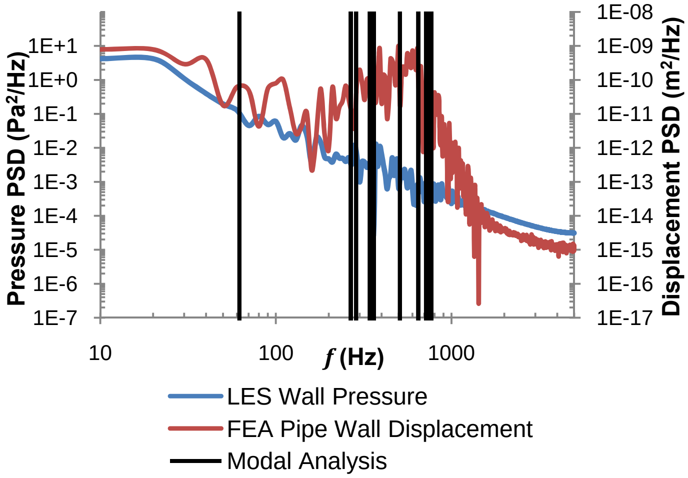


**Figure 9, Long pipe pressure and wall displacement frequency content for *Re* = *1.14x10*$^6$, *D* = 0.1015 m, *t* = 2 mm, *E* = 21 GPa, $\rho_{eq}$ = 3000 kg/m$^3$, $\beta$ = 0.001. Also shown: pipe natural frequencies predicted using a modal analysis**

Any local fluctuations along the wall of the long pipe tend to be small relative to the pronounced large scale bending motions that dominate its response. The pipe tends to respond to an overall net force imbalance that induces deflections similar to those experienced by a beam subjected to a distributed load. Figure 10 shows an image of the deformed long pipe with exaggerated displacement scaling and color contours of displacement magnitude. This bending-beam type of deflection is typical of almost any time step in all of the long pipe solutions.

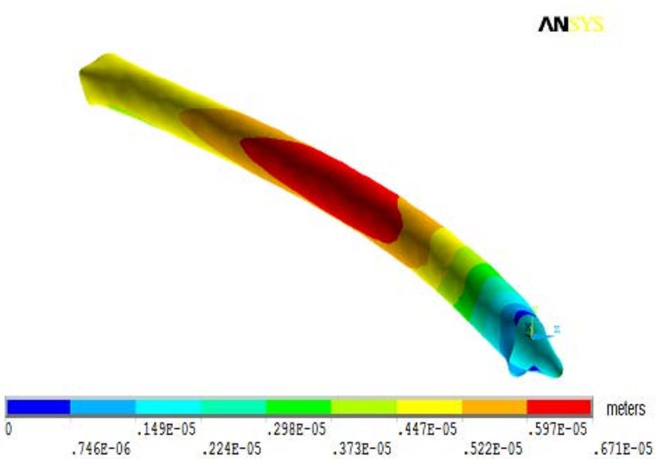


**Figure 10, Long pipe wall displacement pattern for *Re* = *1.14x10*$^6$, *D* = 0.1015 m, *t* = 2 mm, *E* = 21 GPa, $\rho_{eq}$ = 3000 kg/m$^3$, $\beta$ = 0.001**

### *3.3 Non-Dimensionalization*

Dimensional analysis was used to reduce the total number of important variables needed to characterize the problem. The dimensional analysis also gives the results in more generalized form, convenient for comparisons with other work. A complete non-dimensional set of variables accounts for all of the original variables of interest. The dimensionless forms of each of the dependant variables are defined in Table 7.

**Table 7, Dimensionless dependant variables**

| Dimensionless Variable | Definition | Description |
|---|---|---|
| $\delta^*$ | $\frac{\delta'}{D}$ | Ratio of standard deviation of pipe wall displacement to internal diameter |
| $V^*$ | $\frac{V'}{U}$ | Ratio of standard deviation of pipe wall velocity to average fluid velocity |
| $A^*$ | $\frac{A't}{U^2}$ | Dimensionless pipe wall acceleration |

Before defining the dimensionless form of the independent variables it is useful to introduce two new variables. The first represents a characteristic frequency of the fluid flow and is defined as $\omega_c = U/D$, and indicates the lowest frequency of coherent structures expected to be present in the turbulent flow field [21]. The second variable is proportional to the fundamental natural frequency of the pipe in bending [22]. It is defined as $\omega_n = \sqrt{(E/\rho_{eq})} * D/L^2$, where $\rho_{eq}$ is the fluid loaded pipe mass divided by the pipe wall volume. The nine independent variables considered were: $\mu$ (fluid viscosity), $\rho_f$ (fluid density), $U$ (average fluid velocity), $D$ (inner pipe diameter), $t$ (wall thickness), $L$ (support spacing), $\rho_{eq}$ (equivalent pipe density), $E$ (Young's modulus), and $\beta$ (material damping coefficient). Using the previously defined characteristic frequencies, the dimensionless independent variables are defined in Table 8. The total number of independent variables influencing the pipe motion has been reduced from the original nine, to the six dimensionless independent variables.

**Table 8, Dimensionless independent variables**

| Dimensionless Variable | Definition | Description |
|---|---|---|
| $Re_D$ | $\frac{\rho_f UD}{\mu}$ | Ratio of fluid inertial forces to viscous forces |
| $t^*$ | $\frac{t}{D}$ | Ratio of pipe wall thickness to diameter |
| $L^*$ | $\frac{L}{D}$ | Ratio of pipe length to diameter |
| $\rho^*$ | $\frac{\rho_{eq}}{\rho_f}$ | Ratio of total mass to fluid mass |
| $\omega^*$ | $\frac{\omega_n}{\omega_c}$ | Ratio of pipe frequencies to fluid frequencies |
| $\zeta$ | $\beta\omega_n$ | Damping ratio |

All of the listed dimensionless parameters are considered in determining the behavior of the long pipe, however, because the short pipe is able to respond instantaneously to changes in the pressure field, its motion is independent of the parameters $\rho^*$,$\omega^*$, and $\zeta$. Additionally, the effects of $L^*$ have not been considered for the short pipe because it does not undergo significant bending deformation. The short pipe motion is dependent on $E$, so a dimensionless stiffness was defined as $E^* = E/(\rho U^2)$, and is the ratio of the elastic modulus of the pipe material to twice the dynamic pressure of the fluid. The short pipe response is then a function of three variables, namely $Re_D$, $t^*$, and $E^*$.

### *3.4 Complete Functional Relationships*

Each of the dimensionless independent variables was varied one at a time, while holding the others constant, to determine their first order influence on the dimensionless independent variables. $Re_D$ was varied over a range of 9.1x10$^4$ – 1.14x10$^6$, $t^*$ was varied over a range of 9.9x10$^{-3}$ – 7.9x10$^{-2}$, $L^*$ was varied over a range of 13.8 – 23.6, $\rho^*$ was varied over a range of 3.0 – 12.0, $\omega^*$ was varied over a range of 8.9x10$^{-2}$ – 8.9x10$^{-1}$, $E^*$ was varied over a range of 2.3x10$^5$ – 1.3x10$^7$, and $\zeta$ was varied over a range of 4.7x10$^{-2}$ – 9.3x10$^{-1}$. The first order effects were found to be approximately described by a power-law type relationship of the form $D^* \propto A_i^{n_i}$, where $D^*$ represents any one of the dependant variables, $A_i$ is the $i$th independent variable and $n_i$ is the $i$th power-fit exponent. Each of the variable dependencies were fit with a curve of this form to determine the $n_i$ values of the best power-law fit to the data. Table 9 shows the $n_i$ values for each combination of dependant and independent variables. Table 10 shows the average relative error of the curve fit to the data for each variable combination.

**Table 9, Power-Law Fit Exponents for Each Variable**

| Variable | Short Pipe $n_i$ | | | Long Pipe $n_i$ | | |
|---|---|---|---|---|---|---|
| | δ* | V* | A* | δ* | V* | A* |
| $Re_D$ | -0.26 | -0.30 | -0.38 | -0.20 | -0.12 | -0.18 |
| $t^*$ | -2.05 | -1.96 | -0.90 | -1.16 | -1.06 | +0.04 |
| $L^*$ | - | - | - | -0.72 | -0.34 | -0.16 |
| $\rho^*$ | - | - | - | -1.00 | -1.00 | -1.00 |
| $E^*$ or $\omega^*$ | -1.00 | -1.00 | -1.00 | -1.81 | -0.67 | +0.10 |
| $\zeta$ | - | - | - | -0.22 | -0.51 | -0.35 |

**Table 10, Relative Error of Power-Law Fit for Each Variable**

| Variable | Short Pipe $n_i$ | | | Long Pipe $n_i$ | | |
|---|---|---|---|---|---|---|
| | δ* | V* | A* | δ* | V* | A* |
| $Re_D$ | 10.8% | 6.3% | 11.1% | 5.2% | 6.2% | 8.0% |
| $t^*$ | 3.8% | 1.9% | 1.4% | 5.4% | 3.4% | 0.7% |
| $L^*$ | - | - | - | 3.9% | 1.9% | 2.4% |
| $\rho^*$ | - | - | - | 0.0% | 0.0% | 0.0% |
| $E^*$ or | 0.0% | 0.0% | 0.0% | 7.9% | 12.5% | 4.5% |
| $\zeta$ | - | - | - | 2.8% | 3.6% | 4.6% |

Multiplying each of the independent variables raised to the appropriate power results in a complete predictor of the dependant variable in terms of all independent variables. The results of all of the simulations are compared to the complete functional relationship and plotted. A plot of $\delta^*$ versus its complete functional relationship including all independent variables for the short pipe model is shown in Fig. 11 along with a linear fit line having average relative error of 14%. A plot of $V^*$ versus its complete functional relationship including all independent variables for the short pipe model is shown in Fig. 12 along with a linear fit line having average relative error of 11%. A plot of $A^*$ versus its complete functional relationship including all independent variables for the short pipe model is shown in Fig. 13 along with a linear fit line having average relative error of 21%. A plot of $\delta^*$ versus its complete functional relationship including all independent variables for the long pipe model is shown in Fig. 14 along with a linear fit line having average relative error of 7.6%. A plot of $V^*$ versus its complete functional relationship including all independent variables for the long pipe model is shown in Fig. 15 along with a linear fit line having average relative error of 6.3%. A plot of $A^*$ versus its complete functional relationship including all independent variables for the long pipe model is shown in Fig. 16 along with a linear fit line having average relative error of 6.3%. All of the full data sets are fit very well by straight lines intercepting the origin as expected.

The full functional relationships represented on the x-axis of each of these plots constitute the most important contribution of this research. These relationships describe the first-order contribution of each of the variables explored. Higher order interactions between variables are not represented in the functional relationships presented here.

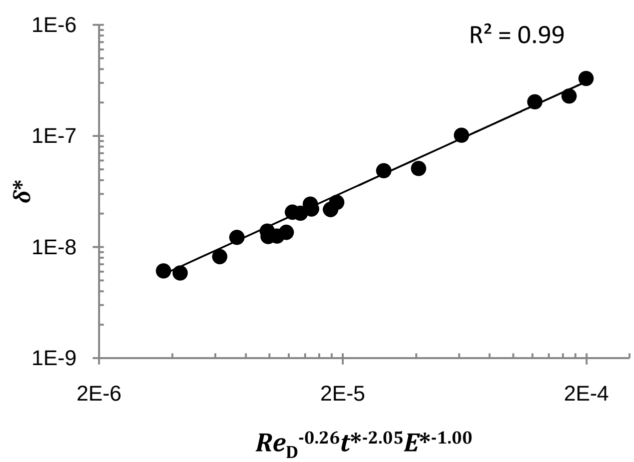


**Figure 11, $\delta^*$ as a function of $Re_D^{-0.26} t^{*-2.05} E^{*-1.00}$ for all short pipe model results**

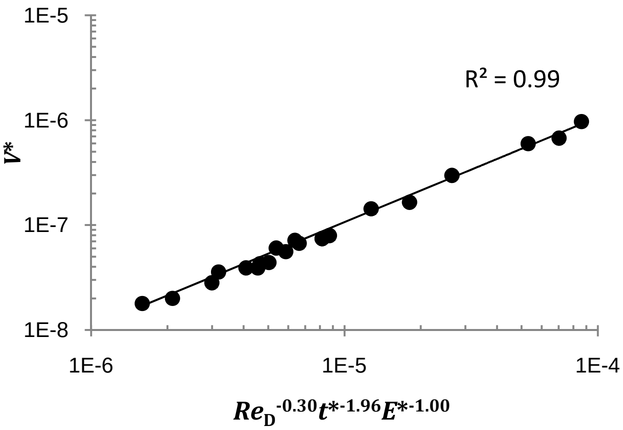


**Figure 12, $V^*$ as a function of $Re_D^{-0.30}t^{*-1.96}E^{*-1.00}$ for all short pipe model results**

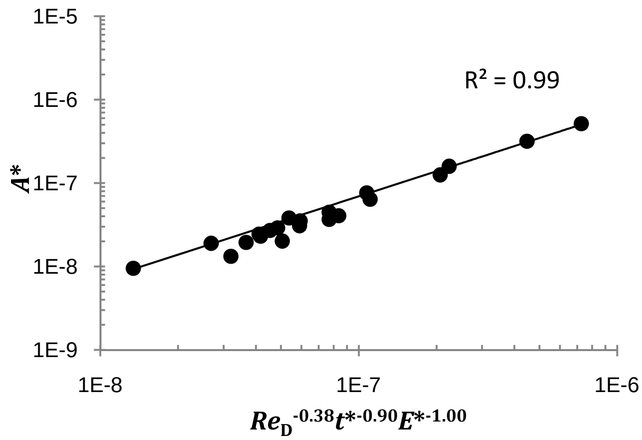


**Figure 13, $A^*$ as a function of $Re_D^{-0.38}t^{*-0.90}E^{*-1.00}$ for all short pipe model results**

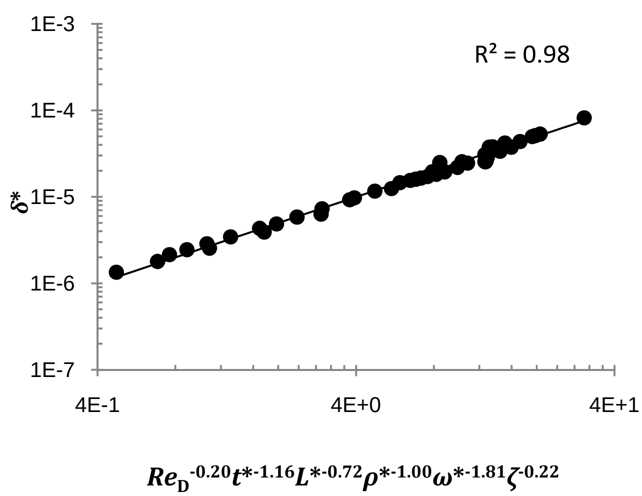


**Figure 14, $\delta^*$ as a function of $Re_D^{-0.20}t^{*-1.16}L^{*-0.72}\rho^{*-1.00}\omega^{*-1.81}\zeta^{-0.22}$ for all long pipe model results**

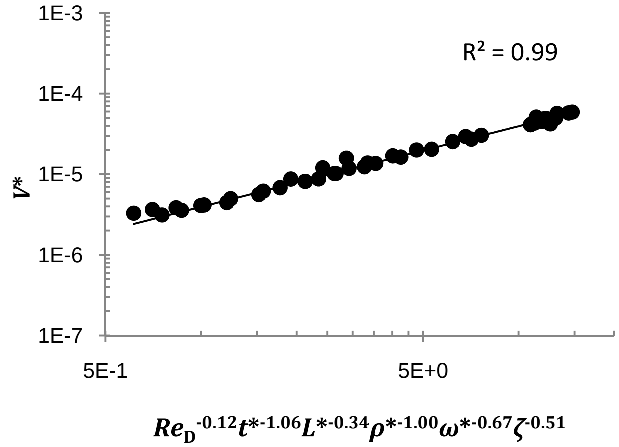


**Figure 15, $V^*$ as a function of $Re_D^{-0.12}t^{*-1.06}L^{*-0.34}\rho^{*-1.00}\omega^{*-0.67}\zeta^{-0.51}$ for all long pipe model results**

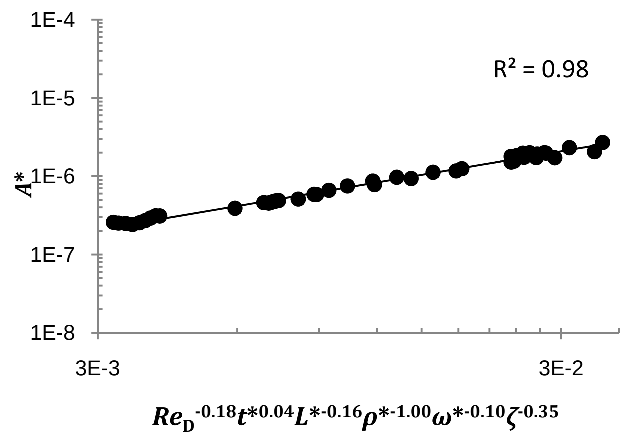


**Figure 16, $A^*$ as a function of $Re_D^{-0.18}t^{*0.04}L^{*-0.16}\rho^{*-1.00}\omega^{*-0.10}\zeta^{-0.35}$ for all long pipe model results**

### *3.5 Comparison with Experimental Data*

There is very little experimental data covering the wide range of variables explored in this research. One of the primary goals of the numerical simulations was to cover a range of variables difficult to explore experimentally. There have, however, been some experimental efforts to characterize turbulent pipe flow induced vibration. Experimental data has primarily explored the effects of varying flow velocity. Additionally, the effects of pipe material and thickness have been explored, but only for two or three different values. Experimental results obtained by Evans predict that pipe wall acceleration is proportional to approximately $U^2$ [12]. Re-dimensionalizing the long pipe results presented in the previous section of this chapter results in a fluid velocity dependence of $A' \propto U^{1.92}$. This is very close to the value predicted by experiment. It should also be noted that all experiments have used pipes with some degree of surface roughness. The effect of surface roughness is to reduce Reynolds number dependence of the wall shear stress. If the wall pressure fluctuations scale with shear stress as indicated by Fig. 5, then the forcing function and pipe wall response would be expected to have less dependence on Reynolds number. Removing the Reynolds number dependence (which is small anyway) from the relationships predicted from this research results in a fluid velocity dependence exponent of 2.1 which is in the range of values (1.94 to 2.19) determined by Thompson [23].

Evans explored the use of 3 pipe materials over a range of flow rates from 7,000 to 23,000 g/s with water as the working fluid. The experimental pipes were all 3 inch (0.0762m) nominal diameter schedule 40 pipe made of PVC, aluminum, and stainless steel. Water was used as the working fluid, and the pipe wall acceleration was measured using an accelerometer. Evans indicates that the experimental data from the PVC pipe is fit very well by the relation $A' = 2.98\text{e-}11$ x $Q^2$, where Q is the flow rate in grams per second. The aluminum pipe data is fit by the same curve divided by a constant 1.2, and the steel pipe data is fit by the same curve as the PVC divided by a constant 2.2. Evans proposes multiplying the data by $\sqrt{\rho_P/\rho_f}$, where $\rho_P$ is the pipe material density and $\rho_f$ is the fluid density, to collapse all three sets onto a single curve [12]. The present numerical simulations suggest that multiplying the data instead by $\rho^*$ will also cause the data to collapse since $A^* \propto 1/\rho^*$. Figure 17 shows a plot comparing the method used by Evans with the curve fit generated using the functional relationships from this research. Both methods allow the data to be fit closely by a single curve, although the fit is slightly better with $R^2 = 0.998$ for the method using $\rho^*$, compared to $R^2 = 0.993$ for the method using $\sqrt{\rho_P/\rho_f}$.

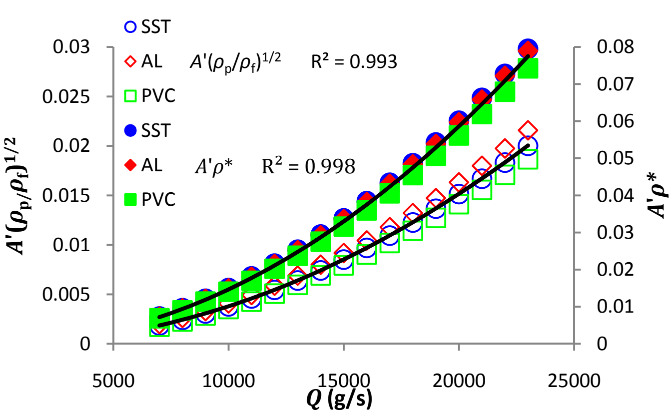


**Figure 17, Comparison of Evans' Method of Data Collapse ($A'(\rho_p/\rho_f)^{1/2}$) to Suggested Method of Data Collapse ($A'\rho^*$) Applied to Evans Experimental Data**

Thompson used only a single pipe material (PVC) for all experiments, but used both schedule 40 and schedule 80 pipe to determine the effects of varying thickness [23]. The pipe wall acceleration was determined using an accelerometer and the fluid velocity was varied by controlling the speed of the driving pump. The PVC test sections were isolated from the pump vibrations by sections of rubber pipe upstream and downstream of the test section. Six sets of data are used here to check the numerical simulation, each corresponding to a different pipe test section. Table 11 shows the geometry of each section used in the experiments performed by Thompson. Water was the working fluid used for all of the experiments.

**Table 11, Thompson experiment pipe geometry**

| Nominal Pipe Size | Pipe Schedule | Inner Diameter, $D$ | Wall Thickness, $t$ |
|---|---|---|---|
| 4 inch | 40 | 0.1023 m | 6.02 mm |
| 4 inch | 80 | 0.0972 m | 8.56 mm |
| 3 inch | 40 | 0.0779 m | 5.49 mm |
| 3 inch | 80 | 0.0737 m | 7.62 mm |
| 2 inch | 40 | 0.0525 m | 3.91 mm |
| 2 inch | 80 | 0.0493 m | 5.54 mm |

The numerical simulations suggest that $A'$ should be nearly inversely proportional to $t^*$ because $A^* \propto t^{*0.04}$. Including the effects of varying $t^*$ and varying $\rho^*$ (which also changes with thickness) while neglecting the influence of Reynolds number, results in the prediction that $A' \propto U^{2.1}/(\rho^* t^{*0.96})$. A plot of the standard deviation of the pipe wall acceleration verses this prediction expression is shown in Fig. 18. The data for each nominal pipe size is fit with a line passing through the origin resulting in a coefficient of determination of $R^2 = 0.95$ for the 4 inch pipe data, $R^2 = 0.98$ for the 3 inch data, and $R^2 = 0.93$ for the 2 inch data. Each pair of data sets (schedule 40 and schedule 80) collapses to nearly a straight line when accounting for changes in pipe wall thickness and average fluid velocity.

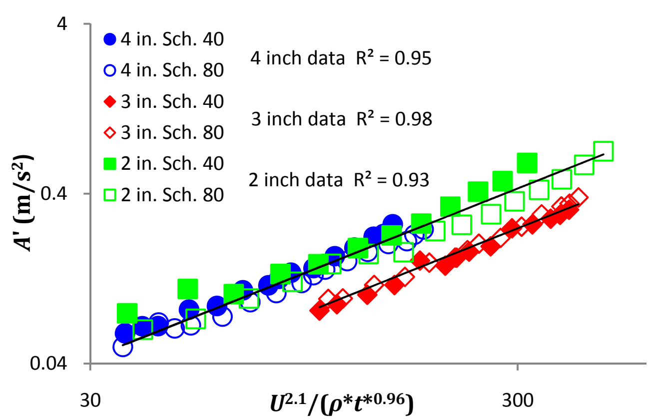


**Figure 18, $A'$ vs. $U^{2.1}/(\rho^* t^{*0.96})$ for Thompson Experimental Data Exhibiting Power-Law Dependency Predicted by Present Numerical Simulations**

The relations developed using the numerical model are able to fit the available experimental data, although it is difficult to account for differences in pipe support boundary conditions, effective pipe length and structural damping in an experiment. The inherent strength of the numerical model is the ability to control these additional parameters independently.

## CONCLUSION

A numerical model of fully developed turbulent pipe flow based on LES has been developed and solved for 8 different Reynolds numbers. The LES model has been verified and validated to ensure accuracy of the solutions obtained through its implementation. The solutions from this fluid model have been used to approximate the fluctuating pressure fields on the inside surface of a pipe. These fluctuating pressure fields have then been applied as external loads on the surface of a structural model of a segment of pipe. The structural model using FEA has also been verified and validated. The magnitude of the pipe wall motion due to the applied pressure fields has been explored for a range of pipe geometric and material property variables. A complete set of non-dimensional parameters that represents all of the variables explored has been used to generalize the results.

The results indicate that there is a fundamental difference in the response of a short pipe compared to the response of a long pipe. The short pipe responds immediately to changes in the pressure field and does not require the pipe inertia to be considered. The short pipe tends to respond to local pressure variations and is more sensitive to changes in wall thickness than a long pipe. The short pipe model indicates reduced response to higher frequencies in the pressure fluctuations which correspond to smaller turbulence length scales. The long pipe model is influenced by the pipe inertia and must include transient structural effects. The long pipe tends to respond primarily in bending modes. The long pipe also shows decreased response to the highest frequency small-scale pressure fluctuations, but also indicates heightened response at middle frequencies that correspond to the natural frequencies of the pipe.

A functional relationship between three pipe motion dependant variables and six dimensionless independent variables exerting influence has been developed by exploring first order effects of each variable. The results can be summarized by these functional relationships as shown in Table 12. These results were compared to available experimental data, and indicate that the numerical model used here has produced results with behavior similar to experimental results.

**Table 12, Functional relationships: Result summary**

| |
|---|
| Short Pipe |
| $\delta^* \propto Re_D^{-0.26} t^{*-2.05} E^{*-1.0}$ |
| $V^* \propto Re_D^{-0.30} t^{*-1.96} E^{*-1.0}$ |
| $A^* \propto Re_D^{-0.38} t^{*-0.90} E^{*-1.0}$ |
| Long Pipe |
| $\delta^* \propto Re_D^{-0.20} t^{*-1.16} L^{*-0.72} \rho^{*-1.0} \omega^{*-1.81} \zeta^{-0.22}$ |
| $V^* \propto Re_D^{-0.12} t^{*-1.06} L^{*-0.34} \rho^{*-1.0} \omega^{*-0.67} \zeta^{-0.51}$ |
| $A^* \propto Re_D^{-0.18} t^{*+0.04} L^{*-0.16} \rho^{*-1.0} \omega^{*+0.10} \zeta^{-0.35}$ |

## ACKNOWLEDGMENTS

Funding for this research was provided by Control Components Inc. and Genscape Inc.

## REFERENCES

[1]Eisinger, F. L. "Desinging Piping Systems Against Acoustically Induced Structural Fatigue." *Journal of Pressure Vessel Technology* 119 (1997): 379-383.
[2] Evans, R., Wilkins, C., Goodrich, L., Blotter, J. Method and apparatus for measuring the mass flow rate of a fluid. United States Patent 6,412,352. (2002).
[3] Weaver, D. S., Zaida, S., Au-Yang, M. K., Chen S. S., Paidoussis, M.P., and Pettigrew, M.J. "Flow-Induced Vibrations in Power and Process Plant Components - Progress and Prospects." *Journal of Pressure Vessel Technology* 122 (August 2000): 339-348.
[4] Durant, C., Robert, G., Filippi, P., Mattei, P. "Vibroacoustic Response of a Thin Cylindrical Shell Excited by a Turbulent Internal Flow: Comparison Between Numerical Prediction and Experimentation." *Journal of Sound and Vibration* 229 (2000): 1115-1155.
[5] Vassilev, V. M., and Djonderjorov, P. A. "Dynamic Stability of Viscoelastic Pipes on Elastic Foundations of Variable Modulus." *Journal of Sound and Vibration* 297 (2006): 414-419.
[6] Paidoussis, M. P. "The Canonical Problem of the Fluid-Conveying Pipe and Radiation of the Knowledge Gained to Other Dynamics Problems Across Applied Mechanics." *Journal of Sound and Vibration* 310 (2008): 462-492.
[7] Evans, R. P., Blotter, J.D., and Stephens, A.G. "Flow Rate Measurements Using Flow-Induced Pipe Vibration." *Journal of Fluids Engineering* 126 (March 2004): 280-285.
[8] Weyers, P. *The Vibration and Acoustic Radiation of Thin-Walled Cylinders Caused by Internal Turbulent Flow*. PhD Thesis, Pasadena, California: California Institute of Technology, 1959.
[9] Birgersson, F., Finnveden, S., and Robert, G. "Modelling Turbulence-Induced Vibration of Pipes With a Spectral Finite Element Method." *Journal of sound and Vibration* 278 (2004): 749-772.
[10] Bochkarev, S. A., and Matveenko, V. P. "Numerical Study of the Influence of Boundary Conditions on the Dynamic Behavior of a Cylindrical Shell Conveying a Fluid." *Mechanics of Solids* 43 (2008): 477-486.
[11] Pittard, M. T. *Large Eddy Simulation Based Turbulent Flow-Induced Vibration of Fully Developed Pipe Flow*. MS Thesis, Provo, Utah: Brigham Young University, 2003.
[12] Evans, R. P. *Mass Flow Measurement Through Flow-Iduced Pipe Vibration*. PhD Dissertation, Pocatello, Idaho: Idaho State University, 2004.
[13] Kim, B. S. "Analysis of Fluid Induced Vibration of Cryogenic Pipes in Consideration of the Cooling Effect." *Journal of Mechanical Science and Technology* 22 (2008): 2375-2385.
[14] Smagorinsky, J. S. "General Circulation Experiments with the Primitive Equations." *Monthly Weather* 91 (1963): 99-164
[15] Ansys CFX V 11.0 *Users Manual*.
[16] Eggels, J. G. M. *Direct and Large Eddy Simulation of Turbulent Flow in a Cylindrical Pipe Geometry*. PhD Thesis, Delft, The Netherlands: Delft University Press, 1994.
[17] Rudman, M. and Blackburn, H. M. "Large Eddy Simulation of Turbulent Pipe Flow." *Second International Conference of CFD in the Minerals and Process Industries CSIRO*. Melbourne, Australia, 1999. 503-508.
[18] Piomelli, U. "Large-Eddy Simulation: Where We Stand." *Advances in DNS/LES AFSOR*. Ruston, Lousiana, 1997. 93-104.
[19] Guo, J. and Julien, P.Y. "Modified Log-Wake Law for Turbulent Flow in Smooth Pipes." *Journal of Hydraulic Research* 41 (2003): 493-501.
[20] Colebrook, C.F., "Turbulent Flow in Pipes with Particular Reference to the Transition Region Between Smooth and Rough Pipe Walls." *Journal of the Institution of Civil Engineers, Vol. II*. London, 1939. 133-156
[21] Pope, S. *Turbulent Flows*. New York, NY: Cambridge University Press, 2000.
[22] Craig, R.R., and Kurdila, A.J. *Fundamentals of Structural Dynamics*. Hoboken, NJ: John Wiley & Sons Inc., 2006.
[23] Thompson, A. *Experimental Characterization of Flow Induced Vibration in Fully Developed Turbulent Pipe Flow*. MS Thesis, Provo, Utah: Brigham Young University, 2009.

 